J Mater Sci (2011) 46:4971–4979
DOI 10.1007/s10853-011-5414-y

Dynamic constitutive behavior of Hastelloy X under thermo-mechanical loads

Sandeep Abotula · Arun Shukla · Ravi Chona

Received: 3 December 2010 / Accepted: 22 February 2011 / Published online: 11 March 2011

Abstract An experimental investigation has been conducted to study the dynamic constitutive behavior of Hastelloy X (AMS 5754) at room and elevated temperatures under varying rates of loading. A split Hopkinson pressure bar (SHPB) apparatus was used in conjunction with an induction coil heating system for applying dynamic loads at elevated temperatures. Experiments were carried out at different temperatures ranging from room temperature (25 °C) to 1,100 °C at an average strain rate of 5000/s. Room temperature experiments were carried out at varying strain rates from 1000 to 4000/s. The results show that as the strain rate increases from quasi-static to 4000/s, the yield strength increases by approximately 50%. Also, under dynamic loading, the yield stress decreases with temperature up to 700 °C, after which it shows a peak at 900 °C before beginning to decrease again as the temperature is further increased. The Johnson–Cook model was used to predict the dynamic plastic response under varying rates of loading and at different temperatures.

S. Abotula · A. Shukla (✉)
Dynamic Photo Mechanics Laboratory, Department of Mechanical, Industrial & Systems Engineering, University of Rhode Island, Kingston, RI 02881, USA
e-mail: shuklaa@egr.uri.edu

S. Abotula
e-mail: sabotula@my.uri.edu

R. Chona
Structural Sciences Center, Air Vehicles Directorate, US Air Force Research Laboratory, Wright Patterson AFB, OH 45433-7402, USA
e-mail: ravi.chona@wpafb.af.mil

Introduction

Hastelloy X is a nickel-base superalloy that possesses excellent high temperature strength and oxidation resistance. It is widely used in gas turbine operations, petrochemical and in aircraft parts. Due to its high oxidation resistance, it is also used for structural components in industrial furnace applications (http://www.nyk.co.jp/en/products/alloys/heat/hx.html). Thus, it is important to understand the constitutive behavior of this material.

Several researchers in the past have investigated the behavior of Hastelloy X. Lai [1] investigated changes in the hardness and impact toughness at room temperature of Hastelloy X after aging up to 1000 h. The author found that it exhibits age hardening at 540 and 650 °C. The author also observed a slight increase in hardness at 871 °C followed by overaging after 4000 h. Yasuo et al. [2] presented experimental results on the changes in the tensile mechanical properties of Hastelloy X after being used in the liner tube of a HENDEL hot gas duct under high temperature helium gas for about 6000 h. They observed that the 0.2% proof stress and total elongation were slightly decreased when Hastelloy X was exposed to high temperature helium. Static tensile stress–strain curves of Hastelloy X were reported in Mil Handbook 5 h [3]. Swindeman and Brinkman [4] reviewed high temperature mechanical properties for materials including Hastelloy X, used in a pressure vessel using stress–strain curves obtained experimentally. They studied the effect of cold work, chemistry, and heat treatment variations in Hastelloy X. Aghaie-Khafri and Golarzi [5] characterized the hot deformation behavior of Hastelloy X using hot compression tests in the temperature range of 900–1,150 °C and at varying strain rates between 0.001 and 0.5/s. They showed that softening mechanisms, dynamic recovery, and

dynamic recrystallization occurred during hot working. Zhao et al. [6] studied the phase precipitation in Hastelloy X heat treated at 750, 850, and 900 °C for 26 and 100 h. They also provided a TTT (time–temperature–transformation) diagram by combining the new experimental results with the existing literature data. This TTT diagram depicted the presence of $M_{23}C_6$ and σ phases at temperatures <900 °C and μ phase between 800 and 980 °C. Hong et al. [7] performed low cycle fatigue tests of Hastelloy X in the temperature range of 650–870 °C under various strain rates. They found that the Coffin–Manson (C–M) plot was different from those at other temperatures and also the fatigue life significantly decreased at the total strain range less than 0.6%. Krompholz et al. [8] determined J-integral R curves for Hastelloy X up to 660 °C using potential drop technique and showed that there is a decrease in J-integral value at 660 °C. Rowley and Thornton [9] modeled viscoplastic behavior of Hastelloy X using the Bodner Partom unified constitutive model. Static compression experiments were conducted at different temperatures to get the parameters for the model. The model results of Hastelloy X for isothermal uniaxial tensile tests showed good agreement with the experimental stress–strain data.

Based on the careful literature search, it was determined that there is no detailed study of the dynamic characterization of Hastelloy X under thermo-mechanical loading. Hence, this study focuses mainly on the dynamic constitutive behavior of Hastelloy X at room and elevated temperatures.

Material and specimen geometry

The material used in this experimental study is Hastelloy X, supplied by Haynes International. The chemical composition of the material is listed in Table 1 (http://www.nyk.co.jp/en/products/alloys/heat/hx.html). It can be observed from the table that Hastelloy X has high content of Ni, Cr, Fe, and Mo. Three different types of specimens were machined as per the requirement of the experiments. According to ASTM E9-89a, cylindrical specimens with a diameter of 12.7 mm and thickness of 25.4 mm were machined for quasi-static experiments. Specimens, having a diameter of 7.62 mm and thickness of 3.81 mm were used for dynamic characterization at room temperature and specimens with a diameter of 6.35 mm and thickness of 3.175 mm were used at elevated temperatures.

Experimental details

Quasi-static characterization

The quasi-static compression tests were performed using Instron Materials Testing System-5585. ASTM standard E9-89a was followed for the specimen dimensions and testing procedure. Experiments were performed at a compression–extension rate of 1 mm/min and the tests were continued up to a strain of 25%. Molybdenum disulfide was used as a lubricant between the specimen and loading head.

Dynamic characterization

A Split Hopkinson Pressure Bar (SHPB) apparatus was used to study the dynamic behavior of Hastelloy X. The SHPB consists of a striker bar, a solid incident bar and a solid transmission bar, all made out of Maraging steel. Incident and transmission bars have a diameter of 12.5 mm and a length of 1,220 mm. The striker bar is propelled using an air-operated gun. A clay pulse shaper of thickness 2 mm was placed at the impact end of the incident bar as shown in Fig. 1 to improve force equilibrium conditions at the specimen–bar interface. The theoretical details of SHPB can be obtained from Kolsky [10]. The specimen was sandwiched between the incident bar and the transmission bar. Molybdenum disulfide was used as a lubricant between the specimen and the contacting surfaces of the bars to minimize friction.

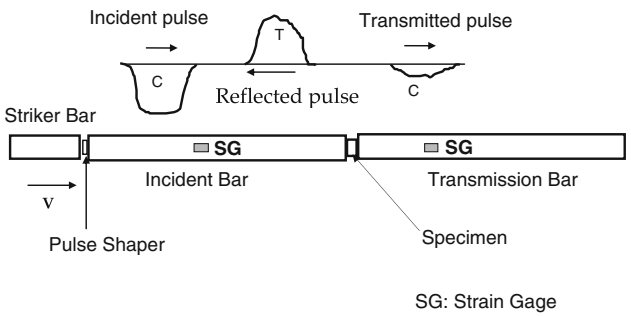

Fig. 1 Experimental setup of SPHB

Table 1 Chemical composition of Hastelloy X (http://www.nyk.co.jp/en/products/alloys/heat/hx.html)

Wt%	C	Si	Mn	P	S	Ni	Cr	Mo	Co	W	Fe	B
Min	0.05	–	–	–	–	–	20.50	8.00	0.5	0.2	17.00	–
Max	0.15	1.00	1.00	0.040	0.030	Residual	23.00	10.00	2.50	1.00	20.00	0.01

When the striker bar impacts the incident bar, an elastic compressive stress pulse, referred to as the incident pulse, is generated. The generated pulse deforms the pulse shaper at the impact end and creates a ramp in the incident pulse which further propagates along the incident bar. When the incident pulse reaches the specimen, part of it reflects back into the incident bar (reflected pulse) in the form of tensile pulse due to the impedance mismatch at the bar–specimen interface and the remaining pulse is transmitted (transmission pulse) to the transmission bar. Axial strain gages mounted on the surfaces of the incident and transmission bar provide time-resolved measures of the elastic strain pulses in the bars.

Room temperature experiments were carried out at strain rates ranging from 1000 to 4000/s. Different strain rates are obtained by varying the velocities of the striker bar. Using one-dimensional wave theory, the true strain and true stress in the specimen can be determined from the reflected and transmitted strain pulses, respectively, as given in Eqs. 1 and 2.

$$\sigma_s = E_b \frac{A_b}{A_s} \varepsilon_t(t) \tag{1}$$

$$\varepsilon_s = \frac{-2c_b}{L_s} \int_0^t \varepsilon_r(t) \mathrm{d}t \tag{2}$$

The expressions for the forces at the specimen incident bar interface and at the specimen transmission bar interface are given in Eqs. 3 and 4, respectively.

$$F_i = A_b E_b (\varepsilon_i + \varepsilon_r) \tag{3}$$

$$F_t = A_b E_b \varepsilon_t, \tag{4}$$

where ε_i, ε_r, and ε_t are the time-resolved strain values of the incident, reflected, and transmitted pulses, respectively, $c_b = \sqrt{E_b/\rho_b}$ is the longitudinal bar wave speed, E_b is the Young's modulus of the bar material, ρ_b is the density of the bar material, L_s is the thickness of the specimen, A_b is the cross-sectional area of the bar, and A_s is the cross-sectional area of the specimen.

Force equilibrium within the specimen during the wave loading is attained when the forces on each face of the specimen are equal. The ratio of these two forces (as given in Eq. 5) provides a measure for force equilibrium. For ideal equilibrium conditions, the ratio should be 1.0.

$$\text{Force ratio,} \quad \frac{F_i}{F_t} = \frac{(\varepsilon_i + \varepsilon_r)}{\varepsilon_t} \tag{5}$$

For experiments at elevated temperatures, the SHPB apparatus in conjunction with the induction coil heating system was utilized as shown in Fig. 2. A special fixture was designed and fabricated to load the specimen. Two

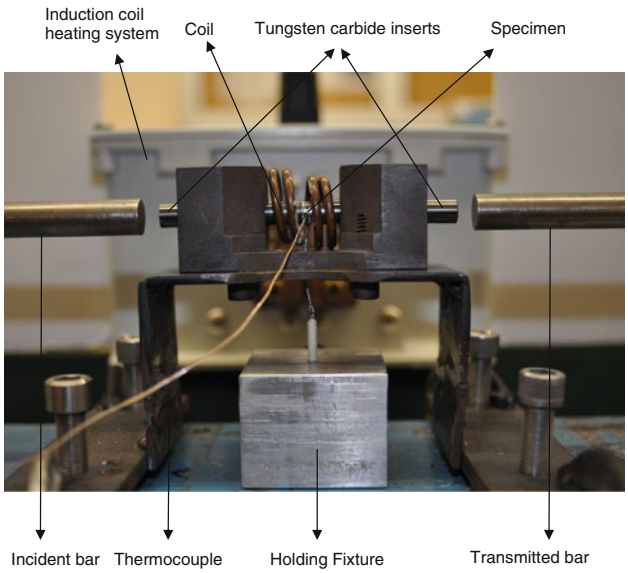

Fig. 2 Experimental setup of SHPB apparatus with induction coil heating system and holding fixture

tungsten carbide inserts were placed between the two pressure bars and the specimen was sandwiched between the tungsten carbide inserts as shown in Fig. 2. The inserts were used to eliminate the temperature gradient in the bars and thus protect the strain gages mounted on them. The impedance of the inserts was matched with the bars; hence they do not disturb the stress wave profiles in the bar. The impedance matching requires the diameter of these tungsten carbide inserts to be smaller than the main pressure bars. This is the reason for the specimen diameter for high temperature testing being smaller than that for room temperature testing. The bars were kept apart initially, later the specimen and carbide inserts were heated in isolation to the desired temperature (usually about 20–50 °C higher than the test temperature) and soon after the bars were brought manually into contact with the specimen. The temperature of the specimen was monitored using a 0.127 mm chromel–alumel thermocouple, which was spot welded onto the specimen. In most of the experiments, it takes <2 min to heat the specimen to the required temperature and it takes <10 s to bring the pressure bars into contact with the tungsten inserts and fire the gun.

High temperature experiments were carried out from room temperature to 1,100 °C under identical strain rate of about 5000/s. Molybdenum disulfide was used as lubricant in the initial experiments and subsequently this was replaced with boron nitride. Molybdenum disulfide works well till about 300 °C and boron nitride is supposed to work till about 1,200 °C. Both the lubricants show about same amount of barreling (1–2% differences in the center diameter to outside diameter).

Johnson–Cook constitutive model

Model description

Johnson and Cook proposed an empirical constitutive model [11, 12] to predict the plastic behavior of metals that are subjected to large strains, high strain rates, and high temperatures. It is one of the most widely used models due to its simplicity and yet effective form. According to the model, the flow stress can be written as

$$\sigma = (A + B\varepsilon_{\mathrm{p}}^{n})\left(1 + C\ln\left(\frac{\dot{\varepsilon}_{\mathrm{p}}}{\dot{\varepsilon}_{\mathrm{o}}}\right)\right)(1 - (T^{*})^{m}), \tag{6}$$

where σ is the flow stress, A and B are the strain hardening parameters and typically A is referred as the yield stress at reference strain rate and reference temperature, C is a dimensionless strain hardening coefficient, ε_{p} is the plastic strain, $\dot{\varepsilon}_{\mathrm{p}}/\dot{\varepsilon}_{\mathrm{o}}$ is the dimensionless strain rate with $\dot{\varepsilon}_{\mathrm{p}}$ being the plastic strain rate and $\dot{\varepsilon}_{\mathrm{o}}$, the reference strain rate. Parameters n and m are power exponents of the strain hardening and thermal softening terms. T^{*} represents normalized temperature as given below in Eq. 7

$$T^{*} = \frac{T - T_{\mathrm{reference}}}{T_{\mathrm{melt}} - T_{\mathrm{reference}}}, \tag{7}$$

where T_{melt} is the melting temperature, $T_{\mathrm{reference}}$ is the reference temperature, and T is the test temperature. The expression in the first set of parentheses in Eq. 6 represents stress as a function of strain, the expression in the second set of parentheses represents the effect of strain rate, and the expression in the third set represents the effect of temperature.

Determination of parameters of model

As shown in Eq. 6, there is a set of five model parameters that need to be identified (A, B, C, n, and m). A, B, and n are obtained from a quasi-static test at room temperature. The parameter A is often defined as the yield stress of the reference strain rate [11]. Here, the quasi-static strain rate is considered as the reference strain rate. Parameter A (yield stress) is determined by considering 0.2% strain offset from the quasi-static test. Once A is determined, parameters B and n are obtained by fitting the quasi-static test data to the model as given in Eq. 8.

$$\ln(\sigma - A) = \left(\ln B + n\ln\varepsilon_{\mathrm{p}}\right) \tag{8}$$

Having identified A, B, and n, the next step is to determine the value of C. Dynamic SHPB experiments at reference temperature and different strain rates are used to estimate the value of C. The initial yield point and strain rate $(\dot{\varepsilon}_{\mathrm{p}})$ from each dynamic test was used to determine C. In doing so, it was ensured that the heat generated from plastic work was not taken into account, thus ignoring the temperature effect. The parameter C for a given dynamic test can be calculated as given in Eq. 9

$$C = \frac{\left(\frac{\sigma}{A + B\varepsilon_{\mathrm{p}}^{n}} - 1\right)}{\ln\left(\frac{\dot{\varepsilon}_{\mathrm{p}}}{\dot{\varepsilon}_{\mathrm{o}}}\right)} \tag{9}$$

The calculated value of C at different strain rates may not be the same due to variations in the experimental data so an average value of C is obtained.

Now the final task is to identify the value of m. A set of experiments at different temperatures but identical strain rate are used to determine the value of m. A similar procedure is followed to that of parameter C, but the effect of temperature is included. As each of the parameters is identified from separate experiments, the final set of parameters may or may not predict the material behavior when all the terms vary at the same time. Therefore, the identified parameters may predict few experiments very well but not other experiments. Hence, it is important to optimize the identified parameters, which can be done by minimizing the average relative error (Δ) between the experimental data and the predicted flow stress [13].

$$\Delta = \frac{1}{N}\sum_{i=1}^{N}\left|\frac{\sigma_{\mathrm{exp}}^{i} - \sigma_{p}^{i}}{\sigma_{\mathrm{exp}}^{i}}\right| \times 100\%, \tag{10}$$

where σ_{exp} is the experimental flow stress, σ_{p} is the predicted flow stress, and N is the total number of data. The Johnson–Cook material parameters of Hastelloy X are shown in Table 2.

Experimental results

Quasi-static response

The true stress versus true stain curve for Hastelloy X under quasi-static conditions is shown in Fig. 3. It has two regions: the initial linear portion and the non-linear portion. The material exhibited yield strength of 380 MPa and Young's Modulus of 190 GPa. The flow stress (strain hardening) of the material increases as the true strain increases.

Table 2 Johnson–Cook material parameters of Hastelloy X

Parameters	A (MPa)	B (MPa)	C	n	m
Value	380	1200	0.012	0.55	2.5

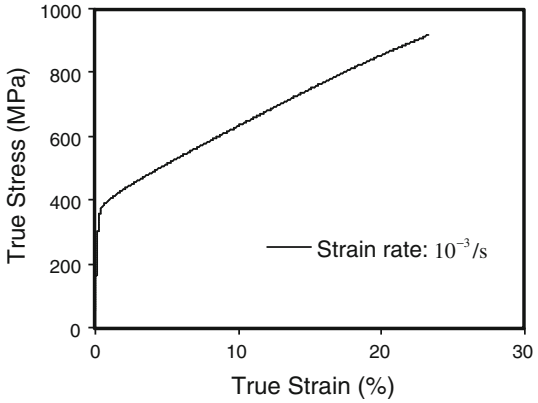

Fig. 3 True compressive stress–strain curve of Hastelloy X under quasi-static loading

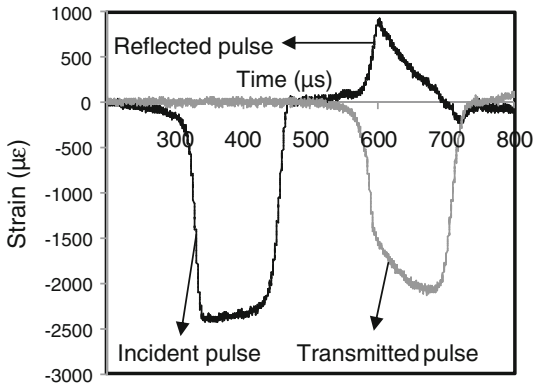

Fig. 4 Typical real-time strain pulses obtained from strain gages mounted on the bars for an average strain rate of 2500/s

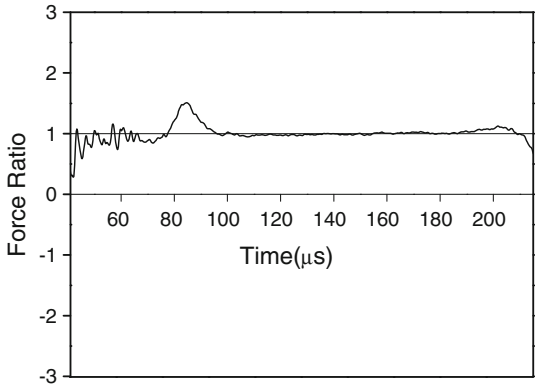

Fig. 5 Typical force equilibrium conditions at the specimen–bar interface at an average strain rate of 2500/s

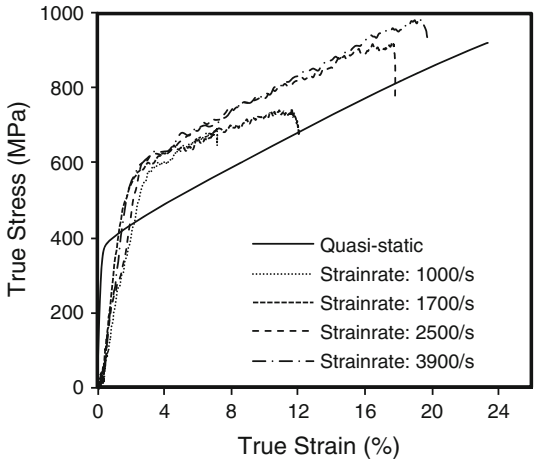

Fig. 6 True compressive stress–strain curve of Hastelloy X under dynamic loading at room temperature

Dynamic constitutive response at room temperature

The real-time strain pulses obtained for Hastelloy X at an average strain rate of 2500/s are shown in Fig. 4. It can be observed from the figure that the clay pulse shaper used in all these experiments helped to reduce high frequency oscillations in the incident stress wave. It is important for the specimen to be in equilibrium under dynamic loading conditions for valid analysis of data. Figure 5 shows the typical force equilibrium conditions at an average strain rate of 2500/s. The solid line in the figure indicates the ideal force ratio of 1.0. The pulse shaper used improved the force equilibrium conditions at the specimen–bar interface. The force equilibrium was attained at around 50 μs and was maintained during the entire loading duration.

The dynamic true stress–true strain curve for different strain rates ranging from 1000 to 4000/s are plotted along with the quasi-static true stress–true strain curve for Hastelloy X at room temperature in Fig. 6. Hastelloy X shows rate dependency from quasi-static loading to dynamic loading. The dynamic yield strength is about 50% higher than the quasi-static yield strength, while the dynamic flow stress is about 200 MPa higher than the quasi-static flow stress. The constituent elements in the material are responsible for the rate sensitivity of Hastelloy X. Under dynamic loading conditions, the material showed small increase in yield strength and flow stress as the strain rate is increased from 1000 to 4000/s.

Dynamic constitutive response at elevated temperatures

A series of experiments were conducted to investigate the dynamic constitutive behavior of Hastelloy X at different temperatures under identical strain rate of about 5000/s. Figure 7 shows the dynamic true stress–strain curves for Hastelloy X at different temperatures. All experiments were carried out with the same striker bar and at the same pressure. Figure 7 clearly shows that as the temperature increases, the yield strength of the material decreases except at temperatures of 900 and 1,000 °C. The true strain

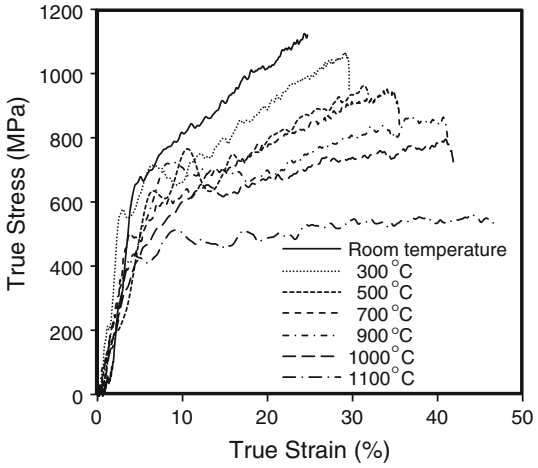

Fig. 7 True compressive stress–strain curve of Hastelloy X under dynamic loading at elevated temperatures and a strain rate of about 5000/s

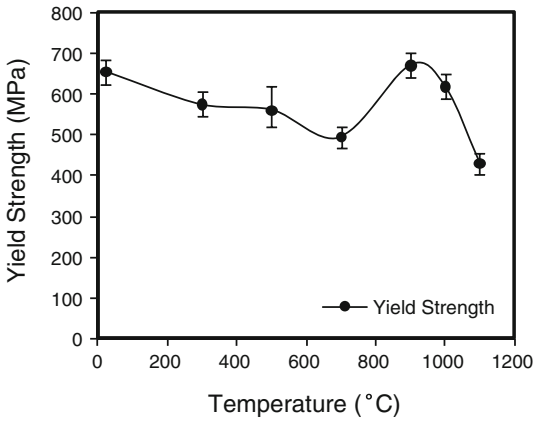

Fig. 8 Effect of temperature on the yield strength under dynamic loading at an average strain rate of 5000/s

in the specimen increases and the flow stress decreases as the temperature increases. As the temperature increases, the material shows more ductile behavior and this result in a decrease in its yield strength and increase in the strain for a given applied stress.

Figure 8 shows the effect of temperature on the yield strength under dynamic loading and the error bars indicate the range of values obtained from three different experiments. As temperature increases, the yield strength decreases initially up to 700 °C, then increases and shows a peak at 900 °C and then again monotonically decreases as the temperature is further increased. The trend reported in this article is in good agreement with the previous findings for Ni-base superalloys [14–19] under quasi-static loadings. Bettge et al. [14] studied the temperature dependence of yield strength of Ni-base superalloy IN 738LC and concluded that the yield strength of the material decreases up to 450 °C, then increases up to 750 °C and finally decreases sharply. Sajjadi et al. [18] observed that the yield strength of GTD-111 under tensile loading decreases with increasing temperature and reaches a minimum value of 750 MPa at 600 °C. With a further increase in temperature to 750 °C, the yield strength increased up to 1,090 MPa and then suddenly decreases. Three important factors were proposed [15, 16, 18] for the behavior of Ni-base superalloys. These are (i) Grain boundary embrittlement, (ii) deformation mechanisms, and (iii) γ' coarsening. Grain boundary embrittlement by carbide particles and deformation mechanisms has almost the same influence on the ductility of these alloys with temperature. The presence of transgranular cracks are more noticeable at higher temperatures but more intergranular cracks can be seen between 750 and 950 °C leading to increase in the yield strength of the material. Also, the ratio of intergranular cracks to transgranular cracks decreases above 950 °C. The transition of crack initiation on the surface from transgranular to intergranular is also noticed in other experiments of Hastelloy X [1, 6, 7, 20]. It was also found that in the tensile properties of Hastelloy X above 950 °C, there is a change in the fracture mode from transgranular dimple rupture to intergranular [2]. For Hastelloy X-280, the presence of M_6C, M_6C', and $M_{23}C$ phases in the 650–930 °C temperature range creates a ductility minimum at those temperatures [21].

Johnson–Cook constitutive model response

As the Johnson–Cook model could only predict the stress in the plastic region, the elastic region was not considered for plotting. The comparison between the experimental data and the predicted data at various strain rates is shown in Fig. 9. A small deviation between the experimental data and the predicted data was observed at all three strain rates and the deviation was more at lower strain rates compared to higher strain rates. The predictability of the Johnson–Cook model for the dynamic plastic response of Hastelloy X was also quantified by calculating average relative error (Δ) and correlation coefficient (R). Average relative error was calculated using Eq. 10 and correlation coefficient (R) can be mathematically expressed as given in Eq. 11 [13].

$$R = \frac{\sum_{i=1}^{N}\left(\sigma_{\exp}^{i} - \bar{\sigma}_{\exp}\right)\left(\sigma_{\mathrm{p}}^{i} - \bar{\sigma}_{\mathrm{p}}\right)}{\sqrt{\sum_{i=1}^{N}\left(\sigma_{\exp}^{i} - \bar{\sigma}_{\exp}\right)^{2}\sum_{i=1}^{N}\left(\sigma_{\mathrm{p}}^{i} - \bar{\sigma}_{\mathrm{p}}\right)^{2}}}, \tag{11}$$

where $\bar{\sigma}_{\exp}$ and $\bar{\sigma}_p$ are the mean values of $\sigma_{\exp}$ and σ_{p}, respectively, and N denotes the number of data points. The correlation coefficient provides information on the strength of linear relationship between the experimental data and the predicted data. The predictability of the model for the

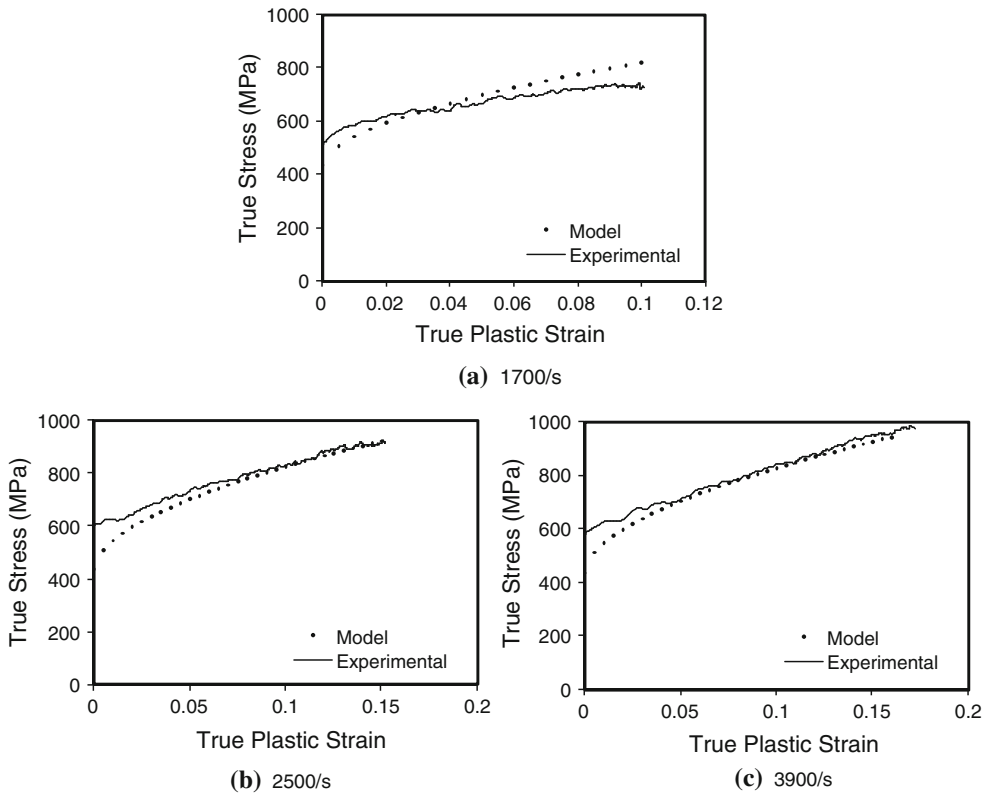

Fig. 9 Experimental data and model prediction of Hastelloy X under dynamic loading at different strain rates

Table 3 Predictability of the model for the dynamic plastic response of Hastelloy X at room temperature under various strain rates

Strain rate (s^{-1})	Correlation coefficient (R^2)	Average relative error (Δ) (%)
1700	0.983	7.24
2500	0.985	2.80
3900	0.987	2.58

dynamic plastic response of Hastelloy X at room temperature under various strain rates is shown in Table 3. There is good correlation between the experimental data and the predicted data for all the three strain rates and the average relative error was low at higher strain rates compared to lower strain rates. Higher value of R^2 (0.985) was observed for strain rate of 2500/s. Even though the value of R^2 (0.983) is high for a strain rate of 1700/s, it has a high relative error (7.24%) which indicates larger deviation between the experimental data and the predicted data. It should be noted that higher value of R^2 may not necessarily indicate better performance [22]. The model has the tendency to be biased toward higher or lower values, whereas Δ is calculated through a term by term comparison of relative error between the experimental data and the predicted data, therefore it produces unbiased statistics. Better correlation can be achieved if the value of Δ is low and this can noticed for a strain rate of 3900/s.

The comparison between the experimental data and the predicted data at different temperatures is shown in Fig. 10. Model predictions for the dynamic plastic response of Hastelloy X at different temperatures are shown in Table 4. The model was not used to predict the dynamic plastic response of Hastelloy X above 700 °C as the material showed different behavior after 700 °C as discussed in the previous section. The model predicted very well for all the three temperatures chosen, with Δ ranging between 2.21 and 6.90%. Excellent correlation between the experimental data and the predicted data was achieved for the temperature of 700 °C and this can be observed in Table 4 showing a low value of Δ (2.21%). Relatively high value of Δ (6.90%) was observed for a temperature of 500 °C.

Conclusions

A series of experiments were conducted to investigate the dynamic constitutive behavior of Hastelloy X at room and elevated temperatures. Clay was used as a pulse shaper in all the experiments to improve force equilibrium conditions

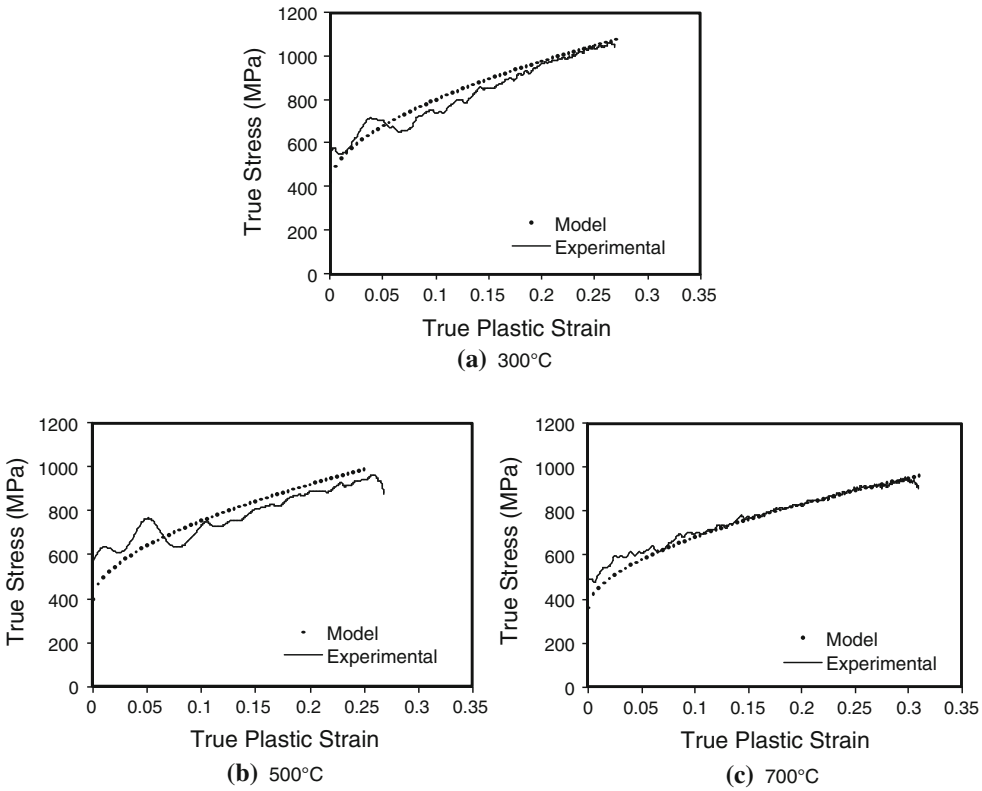

Fig. 10 Experimental data and model prediction of Hastelloy X under dynamic loading at different temperatures

Table 4 Predictability of the model for the dynamic plastic response of Hastelloy X at different temperatures

Temperature (°C)	Correlation coefficient (R^2)	Average relative error (Δ) (%)
300	0.955	4.24
500	0.895	6.90
700	0.989	2.21

at the bar–specimen interfaces. A Johnson–Cook model was used to predict the dynamic plastic response of Hastelloy X under varying strain rates and at different temperatures. Following are the major conclusions of this study:

- Quasi-static experiments showed yield strength of 380 MPa and a Young's Modulus of 190 GPa for Hastelloy X.
- The material showed rate dependency from quasi-static to dynamic loading. An increase of 50% in yield stress and 200 MPa in flow stress was observed from the quasi-static to dynamic loading. Under dynamic loading, the flow stress of the material decreases as the temperature increases.
- The yield strength of the specimen monotonically decreases as the temperature increases up to about 700 °C. Between 700 and 1,000 °C, the yield stress increases before again decreasing as the temperature is further increased.
- The Johnson–Cook model predicted very well for all the experiments and the best correlation was observed for a strain rate of 3900/s ($\Delta = 2.58\%$) in case of room temperatures experiments and for a temperature of 700 °C ($\Delta = 2.21\%$) in case of high temperature experiments.

Acknowledgements The first two authors kindly acknowledge the financial support provided by the Air Force Office of Scientific Research under Grant No. FA9550-09-1-0639. Also the authors would like to thank professor John Lambros for his valuable discussions.

References

1. Lai GY (1978) Metall Mater Trans A 9:827
2. Yasuo K, Kiyoshi F, Kazuhiko K, Yoshiaki M (1988) Metall Mater Trans A 19:1269
3. An unknown copy (1998) Mil-Handbook-5H
4. Swindeman RW, Brinkman CR (1981) In: Technical report, ASME PVP conference, Denver, CO
5. Aghaie-Khafri M, Golarzi N (2007) Mater Sci Eng A 486:641
6. Zhao JC, Larsen M, Ravikumar V (2000) Mater Sci Eng A 293:112
7. Hong HU, Kim IS, Choi BG, Jeong C, Jo Y (2008) Mater Lett 62:4351
8. Krompholz K, Grosser ED, Ewert K (2004) Materialwiss Werkstofftech 13:236
9. Rowley MA, Thornton EA (1996) J Eng Mater Technol 118:19

10. Kolsky H (1949) Proc Phys Soc 62:676
11. Milani AS, Dabboussi W, Nemes JA, Abeyaratne RC (2009) Int J Impact Eng 36:294
12. Johnson GR, Cook WH (1983) In: Proceedings of seventh international symposium on ballistics, The Hague, The Netherlands, pp 541–547
13. Hou QY, Wang JT (2010) Comput Mater Sci. doi:10.1016/j.commatsci.2010.07.018
14. Bettge D, Osterle W, Ziebs J (1995) Scr Metall Mater 32:1601
15. Sajjadi SA, Zebarjad SM (2006) J Achiev Mater Manuf Eng 18:227
16. Sajjadi SA, Zebarjad SM (2006) J Achiev Mater Manuf Eng 28:34
17. Sieborger D, Knake H, Glatzel G (2001) Mater Sci Eng A 298:26
18. Sajjadi SA, Nategh S, Isac M, Zebarjad SM (2004) J Mater Process Technol 155–156:1900
19. Matthews SJ, Greentown, Klein HJ, Hodge FG (1978) US Patent 4129464
20. Petronic S, Milosavljevic A (2007) FME Trans 35:189
21. Claudson TT, Westerman RE (1965) An evaluation of the corrosion resistance of several high temperature alloys for nuclear applications. Metallurgy Research Section, Reactor and Materials Technology Department. AEC Research and Development Report, Atomic Energy Commission
22. Samantaray D, Mandal S, Bhaduri AK (2009) Comput Mater Sci 47:568